ACS Photonics

pubs.acs.org/journal/apchd5

Article

High Contrast, Femtosecond Light Polarization Manipulation in Epsilon-near-Zero Material Coupled to a Plasmonic Nanoantenna Array

Kuidong Wang,* Minghao Li, Hui-Hsin Hsiao, Fengling Zhang, Marcus Seidel, Ai-Yin Liu, Jie Chen, Eloïse Devaux, Cyriaque Genet, and Thomas Ebbesen

Cite This: *ACS Photonics* 2021, 8, 2791−2799

Read Online

ACCESS | Metrics & More | Article Recommendations | Supporting Information

ABSTRACT: Ultrafast manipulation of light polarization is crucial in many nonlinear optic and optoelectronic operations. However, most of the configurations are suffering from low modulation speed (gigahertz) or small contrast ratio. Here, by taking advantange of the anisotropic nonlinear response of indium tin oxide at its epsilon-near-zero region and plasmonic nanoantennas at their polarization-sensitive resonance, we achieve a large, ultrafast anisotropic modulation of light. A polarization elliptic rotation of 32.5° at 1.23 μm wavelength, and a phase delay between the oscillations of the linear polarization axes of $\pi/7$ within 600 fs response time is demonstrated. This approach constitutes a novel, efficient way to implement all-optical high-speed polarization modulators and retarders.

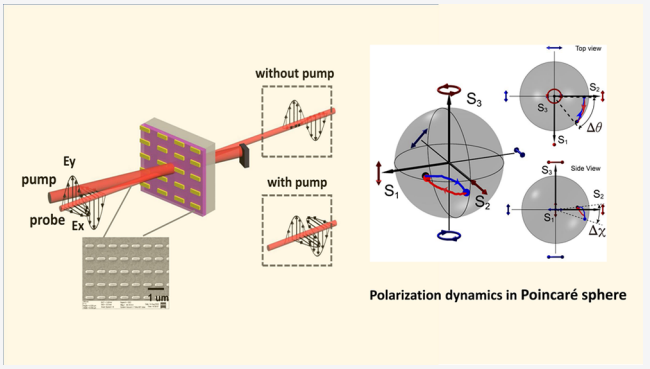

KEYWORDS: *femtosecond optical modulation, polarization manipulation, anisotropic nonlinearity, epsilon-near-zero material, plasmonic nanoantenna array*

Downloaded via UNIV OF BASEL on February 18, 2022 at 16:19:38 (UTC).
See https://pubs.acs.org/sharingguidelines for options on how to legitimately share published articles.

Polarization is a fundamental light property that is applied to split and combine optical fields. To meet the requirements of integrated photonic circuits, active manipulation of light polarization is one of the crucial operations.[1,2] Usually an active polarization component, known as a polarization modulator, can be evaluated by its modulation speed and contrast ratio.[3,4] The modulation speed is mainly determined by the optical or electronic response time of the illuminated material, and the contrast ratio is dependent on the magnitude of its anisotropic nonlinear response. Both azimuthal angle and phase of the polarization state of light will change when the refractive index variations of the material at orthogonal directions are different under external stimuli. Conventionally, the optical polarization is altered significantly by means of electro-optical or magneto-optical effects, such as in Pockels cells and Faraday rotators,[5,6] respectively. However, the modulation time of these usual strategies is typically nanoseconds due to the slow response that comes from control electronics, which severely restricts the application of those modulations in high-speed photonic devices. Ultrafast optical modulation via ultrashort-pulse control paves a promising way for achieving transient modulation of light polarization. These transient optical modulation can be realized in various materials, including metals,[7−9] semiconductors,[10−14] metal−semiconductor hybrid systems,[15,16] 2D materials,[17−19] and organic materials.[20−22] With this in mind, a variety of methods operating in visible,[23−25] near-infrared,[26−28] and terahertz[29,30] regions have been reported for polarization modulation, most of which have response times longer than picoseconds. Although extremely fast polarization control of X-ray radiation in attoseconds has been presented very recently,[31] realizing a femtosecond and large-contrast modulation of polarization in the visible and telecom wavelength ranges remains challenging.

Transparent conducting oxide, such as indium tin oxide (ITO), coupled to nanoantennas has been recently identified as a promising system for nonlinear phase modulation.[32] In this work, the authors strongly coupled the plasmonic mode to an epsilon-near-zero (ENZ) mode that could only be supported by a 23 nm thick ITO layer that is much thinner than the skin depth of ITO[33] and observed a remarkable static phase shift through Z-scan measurements. Here, in contrast, we couple a 310 nm thick ITO film (no ENZ mode) to plasmonic antennas, where no strong coupling between the two modes exists, and investigate the transient optical

Received: June 29, 2021
Published: September 6, 2021

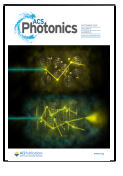

© 2021 American Chemical Society

https://doi.org/10.1021/acsphotonics.1c00971
ACS Photonics 2021, 8, 2791−2799

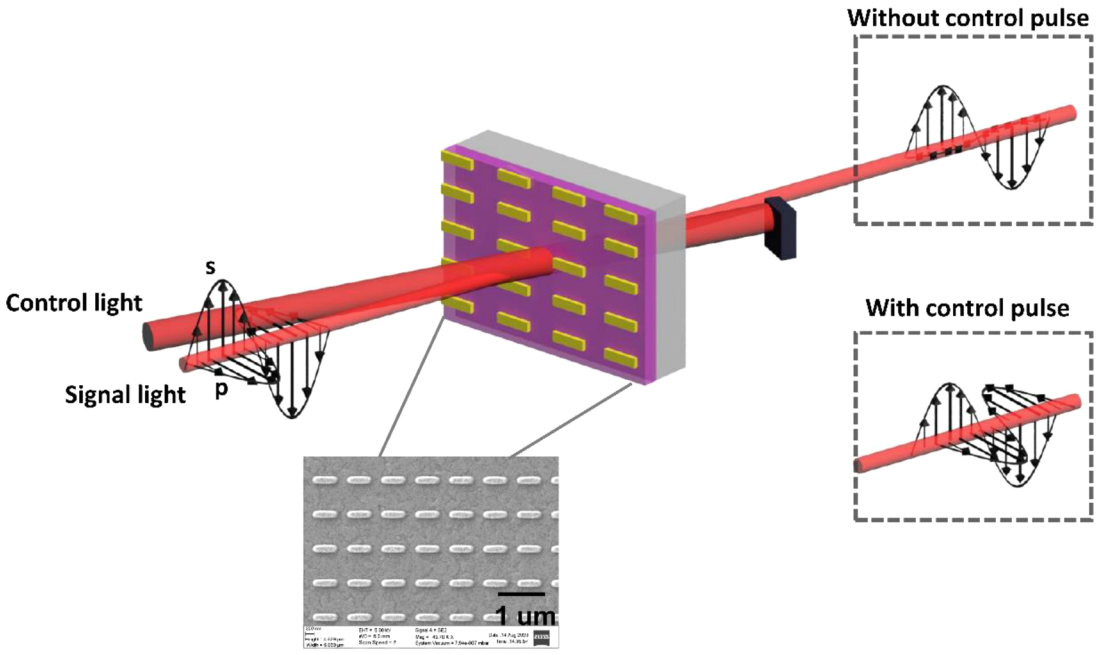

Figure 1. Femtosecond polarization modulation configuration. Schematic of the femtosecond manipulation of the polarization state of light. The transmitted signal light is dominated by *s*-polarized component (direction perpendicular to the length of antennas) when no control light is illuminated and becomes elliptical polarized due to the pump-induced phase delay and transparency of the *p*-polarized component under control excitation. Inset: the SEM image of the gold nanoantennas.

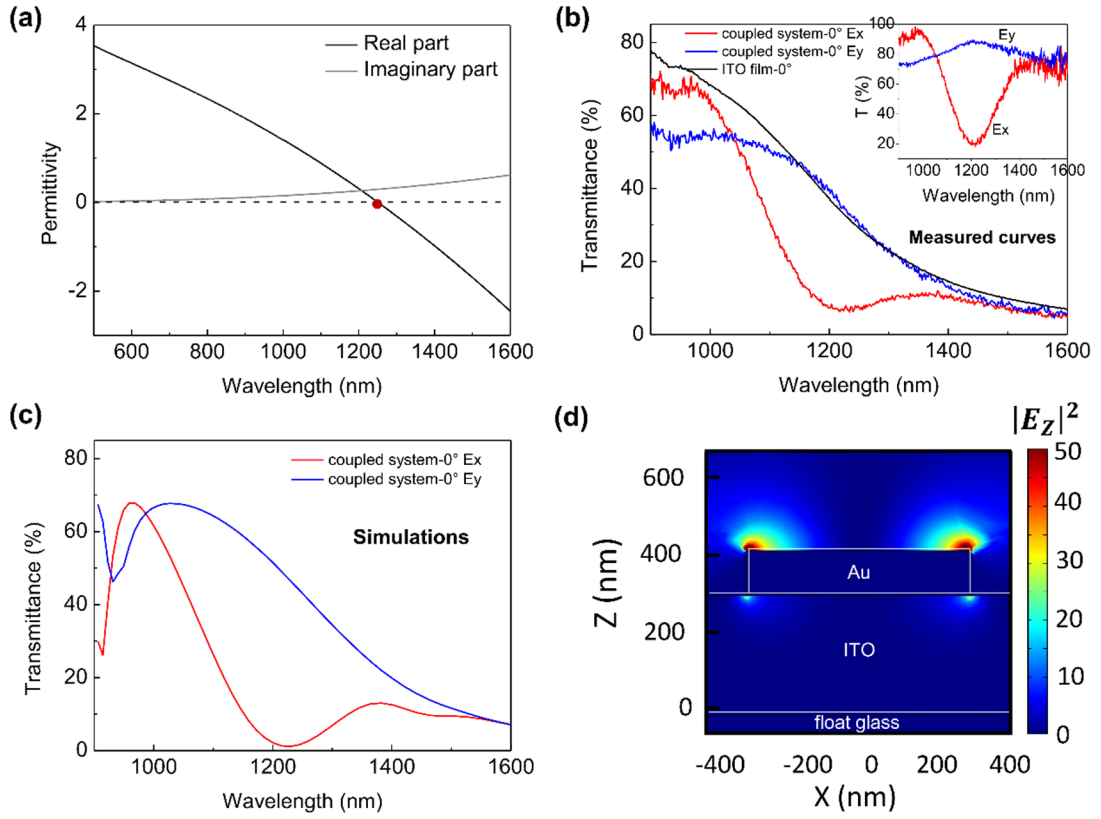

Figure 2. Linear optical responses of the ITO-antennas coupled system. (a) Real (black curve) and imaginary (gray curve) parts of the permittivity of ITO film used in this study. ENZ wavelength is indicated by a red dot. (b) Linear transmittance spectra of the ITO film (black curve) and the coupled system for *Ex*- (red curve) and *Ey*-polarization (blue curve) at the normal incidence. Inset, transmittance spectra of the nanoantennas at the normal incidence when taking the ITO film as the baseline. (c) Simulated transmittance spectra of the coupled system calculated by the finite-element method (COMSOL Multiphysics). (d) Electric field intensity distribution of the coupled system at the resonant wavelength of 1230 nm. Here, only one antenna is shown.

https://doi.org/10.1021/acsphotonics.1c00971
ACS Photonics 2021, 8, 2791−2799

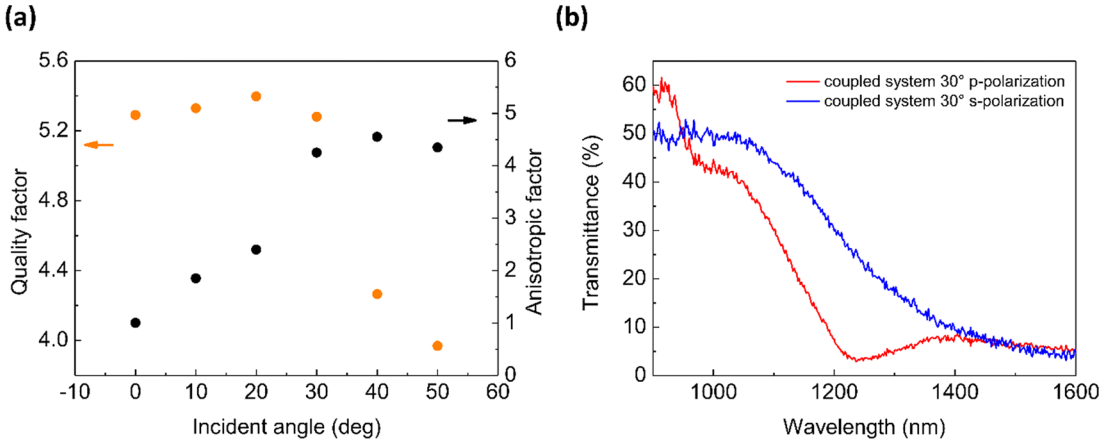

Figure 3. (a) Quality factor of plasmonic resonance (orange circles) and anisotropic factor of the ITO film (black circles) as a function of the incident angle. (b) Linear transmittance spectrum of the ITO-antenna coupled system for *p*- (red curve) and *s*-polarization (blue curve) with an incident angle of 30°.

dynamics that can be induced from very strong polarization and phase changes on subpicosecond time scales that lead to large modulated optical responses offered by such coupled system. More precisely, by combining the large anisotropic nonlinearity of a thick ITO film at its ENZ region and plasmonic nanoantennas at their polarization-sensitive resonant wavelength (λ_{SP}) and by applying ultrafast optical pump−probe technique, we not only obtain a pronounced transient phase change ($\pi/7$), but importantly achieve a significant polarization rotation (32.5°) within 600 fs switching time (corresponding to a calculated bandwidth of ∼0.73 THz for Gaussian pulses with a time-bandwidth product of 0.44) when λ_{SP} is close to ENZ wavelength (λ_{ENZ}). As discussed further below, the possibility to reach a femtosecond response of the coupled system stems from the ultrafast electron−electron (e-e) and electron−phonon (e-p) scattering processes together with the large modulation in the polarization state that results from the large anisotropic nonlinearity of the coupled system. Under resonant pumping, hot electrons are excited, and both the plasma frequency of ITO and the plasmonic resonance of the nanoantennas are red-shifted. The transient evolution of the transmitted polarization states and their large modulation in the time domain makes our coupled system particularly appealing for the designing of new transient transmissive polarizers and retarders.

RESULTS AND DISCUSSION

Design Principle. The principle of the femtosecond polarization modulation, based on an ITO-nanoantenna coupled system, is presented in Figure 1. Here, the modulation of the polarization state can be characterized by rotation of the polarization azimuth and the change of the phase. For 45° linearly polarized incident signal light (half *p*-polarized and half *s*-polarized), when there is no external excitation, the coupled system is transparent for the *s*-polarized component and nearly opaque for the *p*-polarized component at the resonant wavelength, due to the polarization selectivity of the plasmonic antennas and the ENZ material at oblique incidence.[13] It thus appears like a transmissive polarizer. Under the femtosecond control pulse excitation, an anisotropic nonlinear response of the coupled system is induced. In such a case, the amplitude modulation along the *p*-polarization direction is much larger than that for *s*-polarization one. The optically excited free-electron oscillations result in a redshift of the ENZ wavelength and the plasmonic resonance. As a result, the coupled system then becomes transparent for both *s*- and *p*-polarized light at λ_{SP}. Therefore, the polarization azimuth of the transmitted light displays a transient rotation. Moreover, the large anisotropic nonlinearity of the coupled system under the control pulse also corresponds to the difference in refractive index along *p*- and *s*-polarized directions, which gives rise to an ultrafast phase change of the transmitted signal light.

Linear Optical Response. The coupled system used in our study consisted of gold nanoantennas on top of a 310 nm thick ITO film. The plasmonic antennas, with average dimensions of 580 nm × 180 nm × 90 nm, were fabricated with a standard electron-beam lithography technique. The dimensions of the unit cell were 800 nm × 800 nm and the details of the sample's preparation are given in Methods. The size and periodicity of the antenna were designed intentionally to support a localized plasmon resonance at the wavelength close to λ_{ENZ} -the optimization of the antenna dimensions are discussed in Supporting Information S1. The linear permittivity of the ITO film was measured using a spectroscopic ellipsometry (M-2000, J.A. Woollam Co. Inc.), and the corresponding zero permittivity (real part) occurs at 1240 nm (λ_{ENZ}), as shown in Figure 2a. The transmittance spectrum of the ITO film and the coupled system for mutually orthogonal polarizations, E_x (direction parallel to the length of the antenna) and E_y, recorded at the normal incidence, are shown in Figure 2b. Here, the reverse-S-shaped transmittance spectrum of the ITO film reveal the characteristic optical property of ENZ materials, that is, those materials exhibiting dielectric-like (high transmittance) or metal-like (high reflectance) properties at the wavelength shorter or longer than their λ_{ENZ}, respectively. In clear contrast with the spectrum measured under E_y incident polarization, a remarkable transmittance dip for the E_x-polarization was observed for the coupled system at 1230 nm, which results from the light absorption at the plasmonic resonance.[34] Here, the resonant wavelength of the nanoantennas can be estimated (1230 nm) by comparing the spectrum of the sole ITO film with the spectrum the coupled system, as shown in inset of Figure 2b. In addition, the measured spectra of the coupled system agree well with the theoretical simulations, shown in Figure 2c. It should be noted here that the transmittance

https://doi.org/10.1021/acsphotonics.1c00971
ACS Photonics 2021, 8, 2791−2799

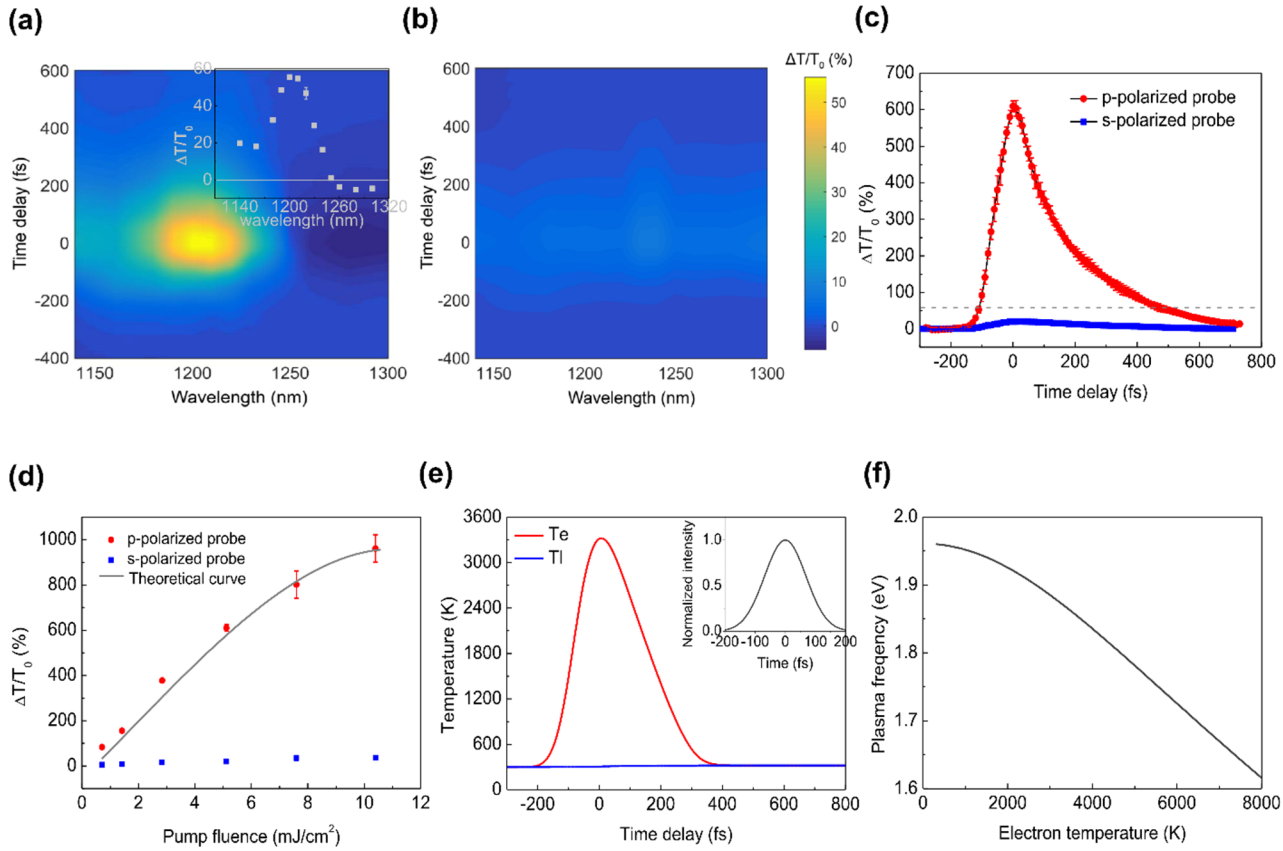

Figure 4. Nonlinear optical amplitude modulation of the ITO-antennas coupled system. Ultrafast amplitude modulation spectrum of the coupled system for (a) *p*- and (b) *s*-polarized signal light under 800 nm nonresonant excitation at a pump fluence of 5.1 mJ/cm^2. Inset of (a): 2D cut of the contour plot at t = 0. (c) Transient optical modulation of the coupled system for *p*- (red dots) and *s*-polarized (blue squares) 1230 nm signal light under 1230 nm resonant excitation at 5.1 mJ/cm^2 irradiated fluence. The dashed gray line (10% of maximal modulation) denotes the baseline when considering the time response. (d) Zero-delay modulation for 1230 nm *p*- (red dots) and *s*-polarized (blue squares) signal light through the coupled system under resonant pumping at various illuminated fluences. Gray curve displays the theoretical values obtained from our model. (e) Temporal response of electron and lattice temperatures of the ITO film under 5.1 mJ/cm^2 fluence calculated from the two-temperature model that is discussed in Supporting Information, S3. Inset: time evolution corresponds to the convolution of the pump- and probe-plasmon-pulse profiles. (f) Electron-temperature-dependent plasma frequency of the ITO based on the nonparabolic conduction band.

amplitude of the E_x-polarized light near the ENZ region shows a discrepancy between the measured and the simulated results. This can be possibly due to fabrication imperfections, surface-roughness-induced scattering, and extra optical loss involved during the fabrication process. From the linear transmittance spectra, we can analyze the electric field distribution of the coupled system. Usually, the transmission is minimized when the light strongly interacts with the dipole antenna and the ENZ layer.[35,36] This leads to enhancement of the electric field on both constituents of the coupled system (Figure 2d). The maximum enhancement factor at the resonant wavelength is ~50 in our case, which is much larger than the value obtained far from the resonance (Figure S1).

The anisotropic nonlinear response of ITO film only occurs at oblique incidence in its ENZ region.[13] Therefore, it is essential to choose the suitable incident angle in our measurements. For simplicity, we use an anisotropic factor to express the ratio of the modulation depth of the *p*-polarized signal light to that of the *s*-polarized signal light when the pump fluence is fixed. As displayed in Figure 3a, when the wavelength of the signal light appears at the ENZ region (1230 nm), the anisotropic factor of the ITO film increases with the incident angle and stabilizes above 30°. Meanwhile, the quality factor of the plasmonic resonance strongly decreases when the incident angle is larger than 30°. Therefore, we set the incident angle of the signal light at 30° to maximize the anisotropic responses of both ITO and nanoantennas. The transmittance spectra of the coupled system for *p*- and *s*-polarized light at 30° are shown in Figure 3b.

Nonlinear Optical Response. We first carried out the amplitude modulation of the transmitted signal light for both *s*- and *p*-polarized cases under both nonresonant (800 nm) and resonant (1230 nm) pump excitations, as presented in Figure 4a–c. The details of the measurements are described in Methods. Here, the modulation depth of the transmitted signal light at a time delay t is defined as the relative change of the static transmittance (T_0) of the coupled system by $\Delta T(t)/T_0 = (T(t) - T_0)/T_0$, and the zero delay is defined at the maximum of the transmittance change. Compared with the less-featured $\Delta T(t)/T_0$ spectrum of the *s*-polarized light, the spectrum of $\Delta T(t)/T_0$ of the *p*-polarized light shows remarkable positive and negative regions centered at 1220 and 1290 nm, respectively, at zero delay under the excitation of a nonresonant pump (Figure 4a,b). Based on the static transmittance spectra (Figure 3b), the absolute transmittance spectra of both *s*- and *p*-polarized signal light at zero delay can be estimated, as indicated in Figure S3. Obviously, this different signs of modulation ascribe to the pump-induced redshift of the

https://doi.org/10.1021/acsphotonics.1c00971
ACS Photonics 2021, 8, 2791−2799

plasmonic resonance of the coupled system. In addition, both modulation regions exhibit similar temporal responses, that is, 200 fs rise time and 300 fs recovery time, which reveal a physical origin related to the thermalization of electrons in the conduction band. For the resonant excitation case, the degenerate pump−probe measurements were investigated, and the recorded results for the different polarized signal beams are displayed in Figure 4c. The amplitude modulation for the *p*-polarized light is 31× larger than that for the *s*-polarized light and also 1 order of magnitude larger than the value measured under nonresonant pump (55%) at the same pump fluence (Figure 4a). An increase of the irradiated fluence will enhance the transmittance variation. In particular, for *p*-polarized signal light, $\Delta T(0)/T_0$ could reach a maximum value of 960% at an illuminated fluence of 10.4 mJ/cm^2 (Figure 4d), which corresponds to the change of the absolute transmittance of the coupled system from 3.6% to 38.2% and to the change of optical density (OD) from 1.44 to 0.42. In comparison, the $\Delta T(0)/T_0$ of the *s*-polarized light is only 37%. This difference shows that the ITO-antennas coupled system exhibits a large anisotropic nonlinearity under resonant excitation. The response time of the modulation (500 fs) resembles that of the nonresonant pump, indicating the same nature of these ultrafast processes.

Under the resonant pump, the physical origin of the ultrafast, large modulation of the transmittance of the signal light is attributed to the femtosecond time evolution and the pump-induced permittivity change of the ITO−antennas coupled system. In order to simplify the discussion, the temporal response and the permittivity variation of the ITO and gold nanoantennas are analyzed separately in the following text.

Because the optical properties of ITO resemble those of a free electron gas at near-infrared wavelengths, the ultrafast response of the ITO can be ascribed to the change of the energy distribution of electrons in the conduction band under laser-induced electron thermalization. The dynamics of the hot electrons is essentially driven by electron−electron (e-e) and electron−phonon (e-p) scattering processes, and the corresponding time evolution of the electron and lattice temperatures can be well described by a phenomenological two-temperature model (see details in Supporting Information, S3).[32,37,38] In this model, a large amount of optical energy is first stored in nonthermal electrons instantaneously during the pump illumination. It is then transferred from nonthermal electrons to thermal electrons (hot Fermi distribution) via e-e scattering process within hundreds of femtoseconds.[39,40] After reaching the highest electron temperature (T_e), the hot electrons interact with phonons through e-p scattering, a process that eventually thermalizes the lattice. During this process, T_e is reduced and the lattice temperature increases. Eventually, electrons and lattice reach a thermal equilibrium. As calculated in Figure 4e, T_e possesses an ∼150 fs buildup time and an ∼300 fs decay time, both times consistent with the time-dependent transmittance variations observed on a bare ITO film, as displayed in Figure S4a in Supporting Information, S3. In the gold nanoantennas, localized surface plasmons are excited instantaneously within the pump pulse irradiation and then damped into hot electrons within 13 fs via e-e scattering. As already reported,[41] the optical nonlinear response induced by plasmons is much larger than that caused by the lattice thermalizing process in metallic nanostructures. Therefore, the duration of the pump-induced plasmon pulse determines the time response of the optical nonlinearity of the nanoantennas. The time evolution of the plasmonic nonlinearity, which corresponds to the convolution of the pump- and probe-plasmon-pulse profiles, is calculated to be 161 fs as displayed in inset of Figure 4e (Supporting Information, S3). Much shorter than the time dependence of the bare ITO transmittance, this plasmonic time response is therefore hidden by that of ITO, thereby making the temporal response of the coupled system resembles that of the bare ITO film (Figure S4a).

The fluence-dependent transmittance change (Figure 4d) is a consequence of the change in refractive index (Δn) of the coupled system. Usually Δn is associated with the nonlinear refractive index (n_2) by $\Delta n = n_2 I$, where I is the intensity of the optical fields that illuminated on the sample.[5] Since refractive index is dependent on permittivity, laser-induced Δn in our case stems from the permittivity variation of both ITO and gold nanoantennas. We assume that the permittivity of ITO follows the Drude model, $\varepsilon(\omega) = \varepsilon_b - \omega_p^2/(\omega(1 + i\Gamma\omega))$, where ε_b is the background permittivity, ω_p is the free electron plasma frequency, ω is the frequency of the incident light, and Γ is the Drude damping rate. Usually, the change in the background permittivity, $\Delta\varepsilon_b$, is strongly dispersive. It has a maximal value near the bandgap energy (3.8 eV)[42] and retains a small value at longer wavelengths.[12] In our measurements, the 1230 nm wavelength corresponds to an intraband transition (conduction band), and thus, $\Delta\varepsilon_b$ can be neglected. According to the two-temperature model, the Drude damping rate at highest T_e under an illuminated fluence of 5.1 mJ/cm^2 will increase 1.5× compared with that at room temperature. However, the modification of Γ contributes only marginally to the transmittance variation (∼5.5%), as seen on the calculations performed using a transfer matrix method.[43] Therefore, the large nonlinearity of ITO is mainly caused by the change in the plasma frequency. Usually, the plasma frequency is associated with electron density in the conduction band (n_e) and electron effective mass (m^*) by $\omega_p^2 = n_e e^2/\varepsilon_0 m^*$, where e is the elementary charge and ε_0 is the permittivity of free space. In our experiments, n_e is unchanged for intraband pumping. Therefore, a nonparabolic conduction band, which results in an electron-wavevector-dependent m^*[44] and, consequently, a T_e-dependent ω_p, must be taken into consideration. As presented in Figure 4f, the plasma frequency is reduced when the electron temperature increases (Supporting Information, S4). The red-shift of ω_p at elevated T_e is consistent with the results in Figure S3. Knowing that the absorbed fluence and the zero-delay T_e can be connected by the two-temperature model (Figure S4b), and revisiting the Drude model, one can easily relate the absorbed fluence to $\Delta T/T_0$ of the pure ITO film by means of T-matrix method. The calculated $\Delta T/T_0$ is plotted in Figure S5a, which agrees well with the experimental data.

The Drude model can also be applied to describe the permittivity of the gold nanoantennas. Considering that the frequency of the light in our experiments is much smaller than the plasma frequency of gold (8.9 eV), both the background permittivity and plasma frequency can be taken as constants. Therefore, only the change in the Drude damping rate plays a role in the permittivity variation of the nanoantennas.[8] Similar with the method used in ITO above, from the two-temperature model and the Drude model, we can relate the electron temperature, the change of the Drude damping rate and the permittivity variation of the nanoantennas. By applying a finite-

https://doi.org/10.1021/acsphotonics.1c00971
ACS Photonics 2021, 8, 2791−2799

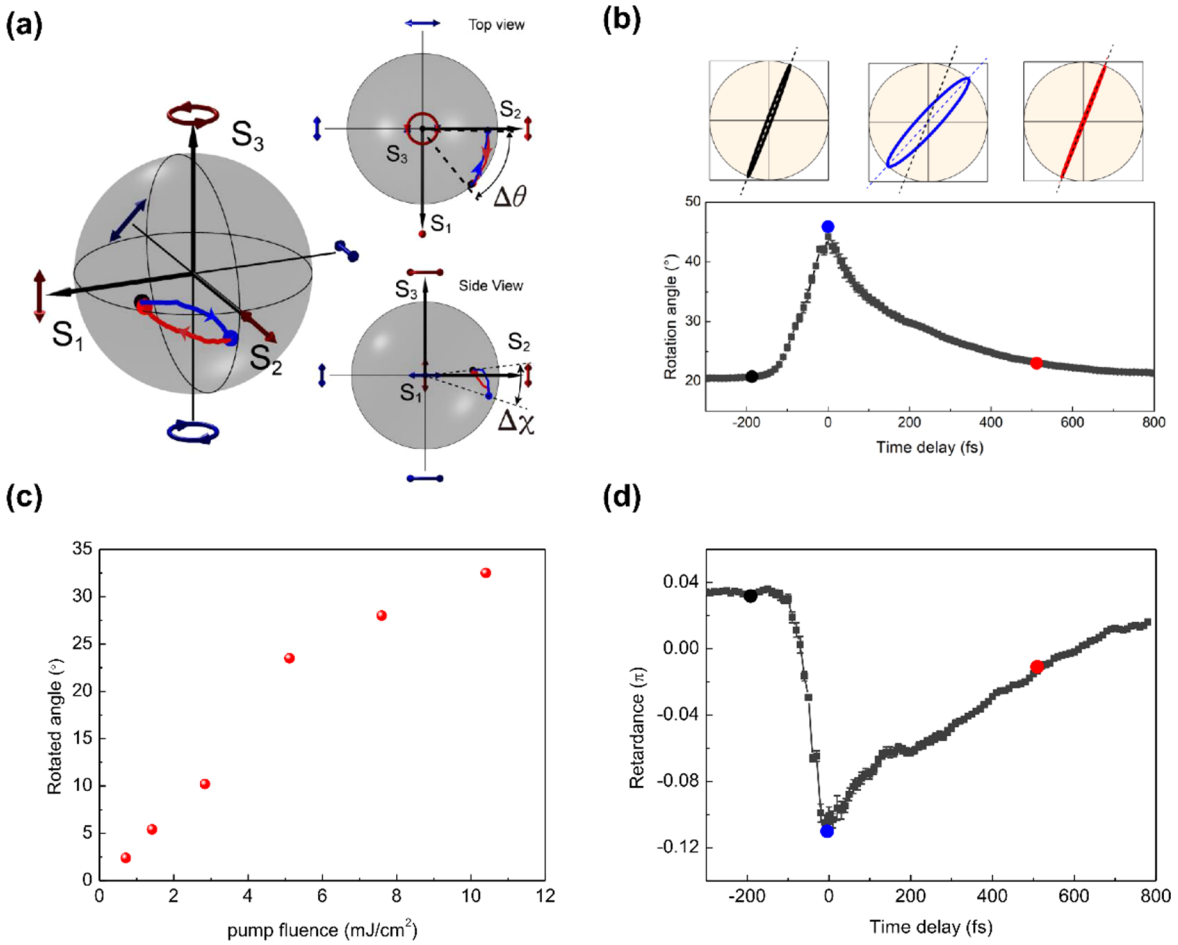

Figure 5. Ultrafast polarization modulation. (a) Dynamics of the polarization state of the transmitted signal light represented in the Poincare sphere. (b) Femtosecond modulation of the polarization azimuthal angle of the signal light through the coupled system under 5.1 mJ/cm^2 resonant excitation. Upper panel shows the polarization ellipse at the corresponding time delay. (c) Rotated angle of the polarization azimuth as a function of irradiated fluence. (d) Temporal response of the retardation between *p*- and *s*-polarized components of the transmitted signal light under 5.1 mJ/cm^2 resonant pump.

element method, meanwhile considering the transmittance variation of ITO as discussed above, the fluence-dependent $\Delta T/T_0$ of the ITO-antennas coupled system for the *p*-polarized signal light can be well estimated, as presented with the gray curve in Figure 4d.

Polarization Modulation. Considering the large anisotropic nonlinear responses described above, it is worth to estimate the polarization state of the transmitted signal light at different time delays between the signal and the control pulses. We do so by putting a rotating quarter waveplate and a fixed polarizer in front of the photodetector (Methods). In our experiments, the incident control light was *p*-polarized and the signal light was linearly polarized at 45°. The wavelength and incident angle of both beams are 1230 nm and 30° (~2° intersection angle), respectively. During the excitation by the control pulse, the polarization state of the transmitted signal light is modified drastically, which persists only for a few hundreds of femtoseconds. This polarization dynamics can be monitored as a trajectory in the Poincare sphere as shown in Figure 5a, where the blue and red lines correspond to the buildup and relaxation processes, respectively. The different paths of the trajectories for these processes reveal different modification mechanisms of the permittivity, where the buildup and relaxation processes correspond to e-e and e-p scatterings, respectively. Analyzing these paths, the S_1OS_2 in-plane angle change corresponds to the change of the azimuthal angle of the polarization state. Furthermore, the polar angle with respect to S_1OS_2 plane represents the change of ellipticity, which is related to the phase difference between *p*- and *s*-polarized components.

The dynamics of the polarization state can also be expressed as the transient change in azimuthal angle and phase. As presented in Figure 5b, prior to the arrival of the control pulse, the transmitted signal light is near-linearly polarized with the azimuthal angle of 20°. Then, a 5.1-mJ/cm^2 control pulse rotates the polarization of the transmitted signal light by 23.5° to reach 43.5°. Finally, the polarization goes back to its initial state within 500 fs. Here, the switching time is more than 1 order of magnitude shorter than that of a plasmonic metamaterial,[23] and nearly 2 orders of magnitude shorter than that at recently reported for a 2D chiral silicon-based split-ring resonator.[27] The fluence-dependence rotation of the polarization azimuth of the transmitted signal light can also be measured in Figure 5c, where the rotated angle increases with the control fluence and eventually reach a maximum of 32.5° at 10.4 mJ/cm^2 irradiated fluence. This trend can be understood by the fact that the anisotropic nonlinearity of the coupled system is enhanced as the pump fluence increases, as indicated

https://doi.org/10.1021/acsphotonics.1c00971
ACS Photonics 2021, 8, 2791−2799

in Figure 4d. In addition, the phase of the transmitted signal light also experiences a transient modification under pump excitation, which makes the transmitted signal light to be elliptically polarized at zero delay (Figure 5b). The phase delay between the oscillations of the linear polarization axes (p- and s-polarized components) increases by $\pi/7$ within 100 fs and goes back to its original state with a response time of ~600 fs (Figure 5d). This transient phase change is mainly caused by the pump-induced distinct refractive indices of the ITO−nanoantenna coupled system at the orthogonal directions. In addition, although the modulation frequency in our measurements is relatively low (1000 Hz), which is determined by the repetition rate of the laser, the temporal response (or switching time) of the ITO−antennas coupled system is an intrinsic property and is independent of laser repetition rate. Therefore, such a high-speed modulation, with a calculated bandwidth of ~0.73 THz, could be used as a promising way to design ultrafast phase retarders.

The polarization-modulation configuration discussed above works at 1.23 μm, it is also possible to extend the operation wavelength to other telecom wavelengths, such as 1.5 μm. A feasible way is to shift the ENZ region of ITO by tuning the carrier concentration/doping.[45,46] Besides, choosing other transparent conducting oxides, such as aluminum-doped zinc oxide, can also achieve the ENZ region at other wavelengths.[47] It should be noted that the power consumption applied here is relative high for realizing practical nonlinear photonic devices. Despite this apparent limitation, we emphasize that the extremely fast response (600 fs) and large modulation contrast achieved in this study still offer an efficient and promising way for realizing ultrafast photonic devices.

CONCLUSIONS

To summarize, by making use of the anisotropic optical nonlinear response of ITO at its ENZ region and nanoantennas at their plasmonic resonances, we have achieved a large anisotropic modulation of p- and s-polarized light in the ITO-antennas coupled system and realized a 32.5° rotation of the light polarization together with a $\pi/7$ phase change within 600 fs. The large anisotropic nonlinearity results from the light-induced redshift of both the plasma frequency of ITO and the plasmon resonance of the nanoantennas, whereas the ultrashort response time of the coupled system stems from the dynamics of hot electrons in conduction band. Such a large anisotropic nonlinearity displayed at the femtosecond scale presented here is promising for high-speed integrated photonic device applications. Moreover, it paves an efficient way for realizing applicable ultrafast polarization modulators and phase retarders.

METHODS

Sample Preparation. The sample used in our measurements is a gold nanoantenna array fabricated on top of a commercially available 310 nm ITO film via standard electron beam lithography (EBL). The ITO film with a sheet resistance of 4.5 Ω/square was deposited on a 1.1 mm float glass substrate. Between the ITO film and the substrate, there is an ~25 nm SiO_2 passivation layer in order to ensure electric insulation. For the EBL process, two layers of the positive PMMA e-beam resists (system 600 K/950 K of AR-P series, Allresist GmbH) were used to improve the accuracy of the exposed pattern. The 600 K and 950 K resists were spin-coated sequentially with a r.p.m. of 4000 and 2000, respectively, on top of the ITO film. The film thickness of the 600 K and 950 K resists were 220 and 100 nm, respectively. After baking the film at 180 °C for 90 s, the designed areas were exposed by 30 keV electron beam (AURIGA, Zeiss). Then, the exposed resist was developed in a conventional solution of methyl isobutyl ketone−isopropyl alcohol (MIBK-IPA) (1:3) for 30 s. To complete the development process, the sample was rinsed with an IPA solution for 30 s. The obtained e-beam resist pattern was used as a mask during evaporating 90 nm gold (0.2 nm/s, PLASSYS ME300). Finally, the gold antenna arrays were achieved by removing the unexposed resist with acetone. The gold antennas, which possess average dimensions of 580 nm × 180 nm × 90 nm, and the unit cell dimension of 800 nm × 800 nm, are designed so that they support localized plasmon modes at 1230 nm (near to ENZ wavelength of ITO) when the polarization of the incident light was parallel to the principal axis of the antennas.

Optical Measurement Setup. The linear transmittance spectra of the ITO and ITO-antennas coupled system for the p- and s-polarized light were measured with a commercial spectrophotometer (Model V-670, JASCO). The ultrafast amplitude modulation was performed with an optical pump−probe setup. The 800 nm light applied here was generated from a Ti:sapphire laser system (Spitfire, Spectra-Physics) that includes a seed laser (Mai Tai, Spectra-Physics) and a Q-switched pump laser (527 nm, Empower, Spectra-Physics). The center wavelength, the pulse width, and the repetition rate of the output of the laser system are 800 nm, 110 fs, and 1000 Hz, respectively. For the nonresonant pump, the 800 nm output beam was split into two portions. Both beams were mechanically modulated at different frequencies. One portion was used as the pump beam, the other was fed into an optical parametric amplifier (OPA, TOPAS) in order to produce tunable near-infrared probe light. The transient transmitted intensity of the probe beam was acquired by a biased InGaAs photodetector (DET10N2, Thorlabs, Inc.). The time delay between the pump and the probe pulses was realized by routing the probe beam through a motorized stage with retroreflectors. The spot diameters of the pump and probe beams were set to 600 and 180 μm, respectively, which ensures a homogeneous pump intensity over the probed area. The probe pulse energy was always set below 0.5 nJ to guarantee a linear response of the photodetector at various incident energies. For the resonant-pump condition, both the pump and probe beams were obtained from the output of the OPA. The pump and probe beams were set to be nearly parallel (~2° intersection angle) and illuminated the sample surface with an incident angle of 30°. This ensured the excitation of localized surface plasmons near the ENZ wavelength.

In order to estimate the Stokes parameters (S_0, S_1, S_2, and S_3) of the polarization state of the transmitted signal light at each time delay, a polarization state analyzer (PSA) consisting of a rotating phase retarder (quarter-wave plate, QWP) and a fixed polarizer were placed in front of the photodetector. Then, for each given angle β of the QWP, the intensity of the transmitted light (I_T) can be written as a function of Stokes parameters,[48] as

$$I_T(\beta, \delta) = \frac{1}{2}\{S_0 + (S_1 \cos 2\beta + S_2 \sin 2\beta)\cos 2\beta - [(S_2 \cos 2\beta - S_1 \sin 2\beta)\cos\delta + S_3 \sin\delta]\sin 2\beta\}$$

https://doi.org/10.1021/acsphotonics.1c00971
ACS Photonics 2021, 8, 2791−2799

where δ is the maximum phase retardation angle, which equals 90° for the QWP used in our measurements. The intensities here were recorded with the retarder rotated to the angles β of 0°, 15°, 30°, 45°, 60°, 75°, 90°, and 105°. This leads to an overdetermined equation system consisting eight equations set for solving four unknown parameters in order to improve the accuracy of the polarization analysis and to minimize random errors on the determination of the azimuthal angle. Since the transmitted signal light from the sample was reflected by two mirrors before entering the PSA, all polarization analysis were corrected by taking into account the polarization response of these mirrors, as explained and analyzed in detail in the Supporting Information, S5.

■ ASSOCIATED CONTENT

Supporting Information

The Supporting Information is available free of charge at https://pubs.acs.org/doi/10.1021/acsphotonics.1c00971.

S1: Linear optical response of various ITO-antennas coupled system; S2: Transmittance spectra of the ITO-antennas coupled system under pump excitation; S3: Modeling the time response of the ITO-antennas coupled system; S4: Modeling the permittivity variation of the ITO-antennas coupled system; S5: Corrections for polarization analysis (PDF)

■ AUTHOR INFORMATION

Corresponding Author

Kuidong Wang − *University of Strasbourg, CNRS, ISIS and icFRC, 67000 Strasbourg, France;* orcid.org/0000-0003-2416-6251; Email: kuidong.wang@unistra.fr

Authors

Minghao Li − *University of Strasbourg, CNRS, ISIS and icFRC, 67000 Strasbourg, France*

Hui-Hsin Hsiao − *Institute of Electro-Optical Engineering, National Taiwan Normal University, Taipei 11677, Taiwan;* orcid.org/0000-0002-9483-8191

Fengling Zhang − *Center for Ultrafast Science and Technology, Key Laboratory for Laser Plasmas (Ministry of Education), School of Physics and Astronomy, Collaborative Innovation Center of IFSA (CICIFSA), Shanghai Jiao Tong University, Shanghai 200240, China*

Marcus Seidel − *University of Strasbourg, CNRS, ISIS and icFRC, 67000 Strasbourg, France;* Present Address: Deutsches Elektronen-Synchrotron DESY, Notkestraße 85, 22607 Hamburg, Germany

Ai-Yin Liu − *Institute of Electro-Optical Engineering, National Taiwan Normal University, Taipei 11677, Taiwan*

Jie Chen − *Center for Ultrafast Science and Technology, Key Laboratory for Laser Plasmas (Ministry of Education), School of Physics and Astronomy, Collaborative Innovation Center of IFSA (CICIFSA), Shanghai Jiao Tong University, Shanghai 200240, China;* orcid.org/0000-0001-5983-7479

Eloïse Devaux − *University of Strasbourg, CNRS, ISIS and icFRC, 67000 Strasbourg, France*

Cyriaque Genet − *University of Strasbourg, CNRS, ISIS and icFRC, 67000 Strasbourg, France;* orcid.org/0000-0003-0672-7406

Thomas Ebbesen − *University of Strasbourg, CNRS, ISIS and icFRC, 67000 Strasbourg, France;* orcid.org/0000-0002-3999-1636

Complete contact information is available at: https://pubs.acs.org/10.1021/acsphotonics.1c00971

Author Contributions

K.W. conceived the idea; H.-H.H. and A.-Y.L. designed the nanostructure and performed the numerical simulations. K.W. fabricated the samples with the help of E.D. and conducted all the optical measurements and the corresponding data analysis with the help of M.L. M.S. extended the pump−probe setup to NIR measurements. K.W., M.L., F.Z., and J.C. did the theoretical part. All authors contributed to discussing and commenting on the manuscript. C.G. and T.W.E. supervised the project.

Notes

The authors declare no competing financial interest.

■ ACKNOWLEDGMENTS

K.W. thanks Yuanyuan Zhang for the help with the permittivity measurements of ITO with the spectroscopic ellipsometer in East China Normal University and Ye Wang (University of Strasbourg) for useful discussions in EBL fabrication. We acknowledge support of the International Center for Frontier Research in Chemistry (icFRC, Strasbourg), the ANR Equipex Union (ANR-10-EQPX-52-01), the Labex NIE Projects (ANR-11-LABX-0058 NIE), CSC (ANR-10-LABX-0026 CSC), USIAS (grant no. ANR-10-IDEX-0002-02) within the Investissement d'Avenir program ANR-10-IDEX-0002-02, ERC (project no. 788482 MOLUSC), PlasHybrid (ANR-18-CE30-0014-02), and QuantERA Project RouTe. M.S. acknowledges support from the Marie Skłodowska-Curie actions of the European Commission (Project 753228, PlaN). H.-H.H. acknowledges support from the Ministry of Science and Technology of Taiwan under the grants MOST 107-2112-M-003-013-MY3 and MOST 110-2112-M-003-020-MY3.

■ REFERENCES

(1) Gansel, J. K.; Thiel, M.; Rill, M. S.; Decker, M.; Bade, K.; Saile, V.; von Freymann, G.; Linden, S.; Wegener, M. Gold helix photonic metamaterial as broadband circular polarizer. *Science* **2009**, *325*, 1513−1515.

(2) Baum, B.; Lawrence, M.; Barton, D., III; Dionne, J.; Alaeian, H. Active polarization control with a parity-time-symmetric plasmonic resonator. *Phys. Rev. B: Condens. Matter Mater. Phys.* **2018**, *98*, 165418.

(3) Reed, G. T.; Mashanovich, G.; Gardes, F. Y.; Thomson, D. Silicon optical modulators. *Nat. Photonics* **2010**, *4*, 518.

(4) Sun, Z.; Martinez, A.; Wang, F. Optical modulators with 2D layered materials. *Nat. Photonics* **2016**, *10*, 227.

(5) Boyd, R. W. *Nonlinear Optics*; Elsevier, 2003.

(6) Crassee, I.; Levallois, J.; Walter, A. L.; Ostler, M.; Bostwick, A.; Rotenberg, E.; Seyller, T.; Van Der Marel, D.; Kuzmenko, A. B. Giant Faraday rotation in single-and multilayer graphene. *Nat. Phys.* **2011**, *7*, 48−51.

(7) MacDonald, K. F.; Sámson, Z. L.; Stockman, M. I.; Zheludev, N. I. Ultrafast active plasmonics. *Nat. Photonics* **2009**, *3*, 55−58.

(8) Wurtz, G. A.; Pollard, R.; Hendren, W.; Wiederrecht, G.; Gosztola, D.; Podolskiy, V.; Zayats, A. V. Designed ultrafast optical nonlinearity in a plasmonic nanorod metamaterial enhanced by nonlocality. *Nat. Nanotechnol.* **2011**, *6*, 107−111.

(9) Ren, M.; Jia, B.; Ou, J. Y.; Plum, E.; Zhang, J.; MacDonald, K. F.; Nikolaenko, A. E.; Xu, J.; Gu, M.; Zheludev, N. I. Nanostructured

plasmonic medium for terahertz bandwidth all-optical switching. *Adv. Mater.* **2011**, *23*, 5540−5544.
(10) Almeida, V. R.; Barrios, C. A.; Panepucci, R. R.; Lipson, M. All-optical control of light on a silicon chip. *Nature* **2004**, *431*, 1081−1084.
(11) Shcherbakov, M. R.; Vabishchevich, P. P.; Shorokhov, A. S.; Chong, K. E.; Choi, D.-Y.; Staude, I.; Miroshnichenko, A. E.; Neshev, D. N.; Fedyanin, A. A.; Kivshar, Y. S. Ultrafast all-optical switching with magnetic resonances in nonlinear dielectric nanostructures. *Nano Lett.* **2015**, *15*, 6985−6990.
(12) Guo, P.; Schaller, R. D.; Ketterson, J. B.; Chang, R. P. Ultrafast switching of tunable infrared plasmons in indium tin oxide nanorod arrays with large absolute amplitude. *Nat. Photonics* **2016**, *10*, 267.
(13) Alam, M. Z.; De Leon, I.; Boyd, R. W. Large optical nonlinearity of indium tin oxide in its epsilon-near-zero region. *Science* **2016**, *352*, 795−797.
(14) Bohn, J.; Luk, T. S.; Tollerton, C.; Hutchings, S. W.; Brener, I.; Horsley, S.; Barnes, W. L.; Hendry, E. All-optical switching of an epsilon-near-zero plasmon resonance in indium tin oxide. *Nat. Commun.* **2021**, *12*, 1−6.
(15) Zhang, X.; Sun, B.; Hodgkiss, J. M.; Friend, R. H. Tunable ultrafast optical switching via waveguided gold nanowires. *Adv. Mater.* **2008**, *20*, 4455−4459.
(16) Abb, M.; Albella, P.; Aizpurua, J.; Muskens, O. L. All-optical control of a single plasmonic nanoantenna-ITO hybrid. *Nano Lett.* **2011**, *11*, 2457−2463.
(17) Li, W.; Chen, B.; Meng, C.; Fang, W.; Xiao, Y.; Li, X.; Hu, Z.; Xu, Y.; Tong, L.; Wang, H.; Liu, W.; Bao, J.; Shen, Y. R. Ultrafast all-optical graphene modulator. *Nano Lett.* **2014**, *14*, 955−959.
(18) Yu, S.; Wu, X.; Chen, K.; Chen, B.; Guo, X.; Dai, D.; Tong, L.; Liu, W.; Ron Shen, Y. All-optical graphene modulator based on optical Kerr phase shift. *Optica* **2016**, *3*, 541−544.
(19) Ni, G. X.; Wang, L.; Goldflam, M. D.; Wagner, M.; Fei, Z.; McLeod, A. S.; Liu, M. K.; Keilmann, F.; Ozyilmaz, B.; Castro Neto, A. H.; Hone, J.; Fogler, M. M.; Basov, D. N. Ultrafast optical switching of infrared plasmon polaritons in high-mobility graphene. *Nat. Photonics* **2016**, *10*, 244−247.
(20) Reichert, M.; Hu, H.; Ferdinandus, M. R.; Seidel, M.; Zhao, P.; Ensley, T. R.; Peceli, D.; Reed, J. M.; Fishman, D. A.; Webster, S.; Hagan, D. J.; Van Stryland, E. W. Temporal, spectral, and polarization dependence of the nonlinear optical response of carbon disulfide. *Optica* **2014**, *1*, 436−445.
(21) Zhao, P.; Reichert, M.; Benis, S.; Hagan, D. J.; Van Stryland, E. W. Temporal and polarization dependence of the nonlinear optical response of solvents. *Optica* **2018**, *5*, 583−594.
(22) Dintinger, J.; Robel, I.; Kamat, P. V.; Genet, C.; Ebbesen, T. W. Terahertz all-optical molecule-plasmon modulation. *Adv. Mater.* **2006**, *18*, 1645−1648.
(23) Nicholls, L. H.; Rodríguez-Fortuño, F. J.; Nasir, M. E.; Córdova-Castro, R. M.; Olivier, N.; Wurtz, G. A.; Zayats, A. V. Ultrafast synthesis and switching of light polarization in nonlinear anisotropic metamaterials. *Nat. Photonics* **2017**, *11*, 628−633.
(24) Taghinejad, M.; Taghinejad, H.; Xu, Z.; Lee, K.-T.; Rodrigues, S. P.; Yan, J.; Adibi, A.; Lian, T.; Cai, W. Ultrafast control of phase and polarization of light expedited by hot-electron transfer. *Nano Lett.* **2018**, *18*, 5544−5551.
(25) Schirato, A.; Maiuri, M.; Toma, A.; Fugattini, S.; Proietti Zaccaria, R.; Laporta, P.; Nordlander, P.; Cerullo, G.; Alabastri, A.; Della Valle, G. Transient optical symmetry breaking for ultrafast broadband dichroism in plasmonic metasurfaces. *Nat. Photonics* **2020**, *14*, 723−727.
(26) Yang, Y.; Kelley, K.; Sachet, E.; Campione, S.; Luk, T. S.; Maria, J.-P.; Sinclair, M. B.; Brener, I. Femtosecond optical polarization switching using a cadmium oxide-based perfect absorber. *Nat. Photonics* **2017**, *11*, 390.
(27) Kang, L.; Wang, C.-Y.; Guo, X.; Ni, X.; Liu, Z.; Werner, D. H. Nonlinear chiral meta-mirrors: enabling technology for ultrafast switching of light polarization. *Nano Lett.* **2020**, *20*, 2047−2055.
(28) Wu, Y.; Kang, L.; Bao, H.; Werner, D. H. Exploiting Topological Properties of Mie-Resonance-Based Hybrid Metasurfaces for Ultrafast Switching of Light Polarization. *ACS Photonics* **2020**, *7*, 2362−2373.
(29) Zhang, Z.; Chen, Y.; Cui, S.; He, F.; Chen, M.; Zhang, Z.; Yu, J.; Chen, L.; Sheng, Z.; Zhang, J. Manipulation of polarizations for broadband terahertz waves emitted from laser plasma filaments. *Nat. Photonics* **2018**, *12*, 554−559.
(30) Cong, L.; Srivastava, Y. K.; Zhang, H.; Zhang, X.; Han, J.; Singh, R. All-optical active THz metasurfaces for ultrafast polarization switching and dynamic beam splitting. *Light: Sci. Appl.* **2018**, *7*, 1−9.
(31) Morgan, J.; McNeil, B. Attosecond polarization modulation of x-ray radiation in a free-electron laser. *Physical Review Accelerators and Beams* **2021**, *24*, 010701.
(32) Alam, M. Z.; Schulz, S. A.; Upham, J.; De Leon, I.; Boyd, R. W. Large optical nonlinearity of nanoantennas coupled to an epsilon-near-zero material. *Nat. Photonics* **2018**, *12*, 79−83.
(33) Campione, S.; Brener, I.; Marquier, F. Theory of epsilon-near-zero modes in ultrathin films. *Phys. Rev. B: Condens. Matter Mater. Phys.* **2015**, *91*, 121408.
(34) Kauranen, M.; Zayats, A. V. Nonlinear plasmonics. *Nat. Photonics* **2012**, *6*, 737.
(35) Schulz, S. A.; Tahir, A. A.; Alam, M. Z.; Upham, J.; De Leon, I.; Boyd, R. W. Optical response of dipole antennas on an epsilon-near-zero substrate. *Phys. Rev. A: At., Mol., Opt. Phys.* **2016**, *93*, 063846.
(36) Kim, J.; Dutta, A.; Naik, G. V.; Giles, A. J.; Bezares, F. J.; Ellis, C. T.; Tischler, J. G.; Mahmoud, A. M.; Caglayan, H.; Glembocki, O. J.; Kildishev, A. V.; Caldwell, J. D.; Boltasseva, A.; Engheta, N. Role of epsilon-near-zero substrates in the optical response of plasmonic antennas. *Optica* **2016**, *3*, 339−346.
(37) Anisimov, S.; Kapeliovich, B.; Perelman, T. Electron emission from metal surfaces exposed to ultrashort laser pulses. *Zh. Eksp. Teor. Fiz* **1974**, *66*, 375−377.
(38) Sun, C.-K.; Vallée, F.; Acioli, L.; Ippen, E.; Fujimoto, J. Femtosecond-tunable measurement of electron thermalization in gold. *Phys. Rev. B: Condens. Matter Mater. Phys.* **1994**, *50*, 15337.
(39) Fann, W.; Storz, R.; Tom, H.; Bokor, J. Direct measurement of nonequilibrium electron-energy distributions in subpicosecond laser-heated gold films. *Phys. Rev. Lett.* **1992**, *68*, 2834.
(40) Fann, W.; Storz, R.; Tom, H.; Bokor, J. Electron thermalization in gold. *Phys. Rev. B: Condens. Matter Mater. Phys.* **1992**, *46*, 13592.
(41) Wang, K.; Chen, L.; Zhang, H.; Hsiao, H.-H.; Tsai, D. P.; Chen, J. Plasmon-enhanced optical nonlinearity for femtosecond all-optical switching. *Appl. Phys. Lett.* **2017**, *111*, 181102.
(42) Hamberg, I.; Granqvist, C. G.; Berggren, K.-F.; Sernelius, B. E.; Engström, L. Band-gap widening in heavily Sn-doped In 2 O 3. *Phys. Rev. B: Condens. Matter Mater. Phys.* **1984**, *30*, 3240.
(43) Katsidis, C. C.; Siapkas, D. I. General transfer-matrix method for optical multilayer systems with coherent, partially coherent, and incoherent interference. *Appl. Opt.* **2002**, *41*, 3978−3987.
(44) Liu, X.; Park, J.; Kang, J.-H.; Yuan, H.; Cui, Y.; Hwang, H. Y.; Brongersma, M. L. Quantification and impact of nonparabolicity of the conduction band of indium tin oxide on its plasmonic properties. *Appl. Phys. Lett.* **2014**, *105*, 181117.
(45) Naik, G. V.; Shalaev, V. M.; Boltasseva, A. Alternative plasmonic materials: beyond gold and silver. *Adv. Mater.* **2013**, *25*, 3264−3294.
(46) Capretti, A.; Wang, Y.; Engheta, N.; Dal Negro, L. Enhanced third-harmonic generation in Si-compatible epsilon-near-zero indium tin oxide nanolayers. *Opt. Lett.* **2015**, *40*, 1500−1503.
(47) DeVault, C. T.; Zenin, V. A.; Pors, A.; Chaudhuri, K.; Kim, J.; Boltasseva, A.; Shalaev, V. M.; Bozhevolnyi, S. I. Suppression of near-field coupling in plasmonic antennas on epsilon-near-zero substrates. *Optica* **2018**, *5*, 1557−1563.
(48) Berry, H. G.; Gabrielse, G.; Livingston, A. Measurement of the Stokes parameters of light. *Appl. Opt.* **1977**, *16*, 3200−3205.

https://doi.org/10.1021/acsphotonics.1c00971
ACS Photonics 2021, 8, 2791−2799